Atmospheric
Measurement
Techniques

Open Access

An assessment of the performance of a 1.5 µm Doppler lidar for operational vertical wind profiling based on a 1-year trial

E. Päschke, R. Leinweber, and V. Lehmann

DWD, Meteorologisches Observatorium Lindenberg-Richard Aßmann Observatorium, Lindenberg, Germany

Correspondence to: E. Päschke (eileen.paeschke@dwd.de)

Abstract. We present the results of a 1-year quasi-operational testing of the 1.5 µm StreamLine Doppler lidar developed by Halo Photonics from 2 October 2012 to 2 October 2013. The system was configured to continuously perform a velocity-azimuth display scan pattern using 24 azimuthal directions with a constant beam elevation angle of 75°. Radial wind estimates were selected using a rather conservative signal-to-noise ratio based threshold of −18.2 dB (0.015). A 30 min average profile of the wind vector was calculated based on the assumption of a horizontally homogeneous wind field through a Moore–Penrose pseudoinverse of the overdetermined linear system. A strategy for the quality control of the retrieved wind vector components is outlined for ensuring consistency between the Doppler lidar wind products and the inherent assumptions employed in the wind vector retrieval. Quality-controlled lidar measurements were compared with independent reference data from a collocated operational 482 MHz radar wind profiler running in a four-beam Doppler beam swinging mode and winds from operational radiosonde measurements. The intercomparison results reveal a particularly good agreement between the Doppler lidar and the radar wind profiler, with root mean square errors ranging between 0.5 and 0.7 m s^{-1} for wind speed and between 5 and 10° for wind direction. The median of the half-hourly averaged wind speed for the intercomparison data set is 8.2 m s^{-1}, with a lower quartile of 5.4 m s^{-1} and an upper quartile of 11.6 m s^{-1}.

1   Introduction

The wind field is one of the most important atmospheric parameters. Its accurate measurement with a high spatial and temporal resolution is crucial for operational numerical weather prediction (NWP) models and it is, of course, also vital for numerous other applications. The operational remote sensing of the vertical wind profile is dominated by radar wind profilers (RWPs), with frequencies ranging from L-band to VHF. Here, the letter codes L and VHF (very high frequency) are standard band designations according to the IEEE standard radar-frequency letter-band nomenclature (Skolnik, 2001). The typical time resolution for wind profiles provided to NWP is currently 30 min.

Recently, a new generation of portable infrared (IR) Doppler lidar (DL) systems based on fibre-optic technology developed for the telecommunications industry has become commercially available. In contrast to conventional DL designs based on free-space optics, the use of fibre-optic elements considerably simplifies fabrication, alignment and long-term stability. While there is currently a large market demand for such systems from the renewable energy sector, it is also interesting to test the capabilities of these new instruments for possible future operational boundary layer wind profiling, complementary to radar profilers.

In particular, the DL may have the potential to measure winds below the height of the first range gate of low-UHF RWP, which is typically on the order of a few hundred metres (about 450 m for the 482 MHz RWP used in this study). This RWP blind zone is due to the constraint of measuring in the far-field of the antenna and finite receiver recovery time. The overlap region between RWP and DL data provides a convenient option for cross-technology calibrations and consistency checks. Finally, the higher vertical resolution of DL data is particularly adequate for wind measurements in the lowest part of the boundary layer.

Previous intercomparisons of DL and RWP winds have generally shown good agreement (Cohn and Goodrich, 2002; Pearson et al., 2009; Shaw et al., 2003). These intercomparisons, however, were always based on temporally short-term measurement periods. For example, Cohn and Goodrich (2002) have shown from a measurement period of 2.3 h that the differences of the Doppler velocities obtained with a 915-MHz boundary layer RWP and the NOAA High Resolution Doppler lidar (HRDL) had a standard deviation of about $\sigma_r = 0.20$–$0.23\,\mathrm{m\,s^{-1}}$, which was attributed to turbulent variability and instrumental noise. A translation of this error into the corresponding error for the horizontal wind resulted in an error of less than 0.11–0.27 m s^{-1} for a 30 min measurement period, depending on the beam pointing sequence (five-beam or three-beam pointing Doppler beam swinging (DBS) configuration). Pearson et al. (2009) compared wind measurements from a 9 min Doppler lidar scan and 10 min averaged 1290 MHz radar data for four different times which also showed a very good level of agreement, except for somewhat less well correlated wind speed data, which was attributed to insects or ground clutter contamination. A month-long field study has been carried out in the Salt Lake Valley (Shaw et al., 2003). Here wind measurements were collected with a 915 MHz RWP and a pulsed DL ($\lambda = 10.59\,\mu$m). Comparisons of half-hour consensus winds obtained with the RWP with corresponding winds from DL using a velocity-azimuth display (VAD) scan pattern showed broad agreement albeit considerable scatter, which was attributed to the different sampling volumes of the two systems.

The article describes the setup and methodology of the test, with a focus on aspects of data processing based on the system's direct output and the results of the comparison statistics derived from about 17 000 wind profiles obtained over the course of a year. To the authors' knowledge, such long time comparisons between a Doppler lidar and radar wind profiler have not been done so far and thus may give valuable and more representative insights into the performance of Doppler lidar wind measurements. The paper is structured as follows: in Sect. 2 the data set used for the analysis is described. It includes information related to instrumentation and, above all, the details of the data processing and quality control. In Sect. 3 the statistics of 1-year-long DL measurements are discussed in comparison to RWP and radiosonde (RS) measurements. An interesting type of "gross error" due to a range ambiguity effect is discussed in Sect. 4. Finally, Sect. 5 presents a summary of the results and conclusions.

2   Data set

The data used for this analysis were obtained at the Lindenberg Meteorological Observatory – Richard Aßmann Observatory (MOL-RAO) from 2 October 2012 to 2 October 2013. At this site, RWP and RS winds are routinely measured and

Table 1. Parameters of the HALO Photonics StreamLine Doppler lidar and the Vaisala/Rohde&Schwarz 482 MHz wind profiler (LAP-16000) installed at the observation site RAO. During the measurement period from 2 October 2012 to 2 October 2013 the two operating parameters (1) total number of pulses averaged and (2) resolution of Doppler velocity have been changed. The values in the brackets are valid starting from 26 July 2013. The wind profiler values for range spacing and dwell time are valid for the "low mode".

	Doppler lidar	Radar wind profiler
Wavelength	1.5 µm	62 cm
Pulse width	160 ns	1000 ns
Range gate length	48 m	94 m
First gate	90 m	450 m
Points per range gate	16	1
Total number of range gates	200	96
Total number of pulses averaged	75 000	507 904 (491 520)
Resolution of Doppler velocity	$\pm 0.0382\,\mathrm{m\,s^{-1}}$	$\pm 0.1195\,(0.1250)\,\mathrm{m\,s^{-1}}$
Telescope focus	800 m	not applicable
Pulse length	25 m	150 m
Total observation time per range gate	320 ns	–
Tange spacing	–	650 ns
Sampling frequency	50 MHz	1.538 MHz
Dwell time	5 s	41.65 s
Nyquist velocity	$\pm 19.4\,\mathrm{m\,s^{-1}}$	$\pm 30.586\,(31.996)\,\mathrm{m\,s^{-1}}$
Number of FFT points	1024	512
Pulse repetition frequency (PRF)	15 kHz	12.195 (12.346) kHz

provided for assimilation into a number of NWP models. Since September 2012, a 1.5 µm DL has been tested with the focus of the capabilities of this measurement system for operational wind profiling within the atmospheric boundary layer (ABL). With a spatial separation of only about 30 m the DL was installed as closely as possible to the RWP to achieve the best possible collocation for the intercomparison. Additionally, four routine radiosonde ascents are carried out on a daily basis with the launch site being about 500 m away from the remote sensing field site. This provides another independent data set of upper-air wind measurements. Obviously, the in situ sampling characteristics of the radiosonde leads to non-optimal collocation and temporal matching for individual data points. Nevertheless, the capability of having three fully independent systems for vertical wind profiling is rather unique.

2.1   Instrumentation overview

In the following, a short description of the set-up and some technical aspects for each of the instruments used is provided.
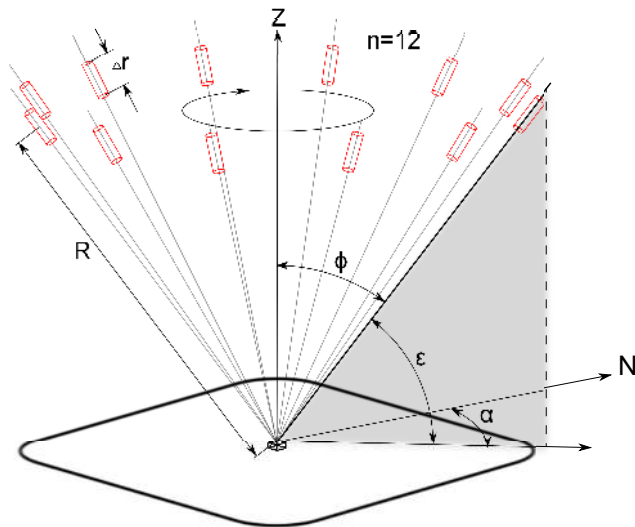
Figure 1. Example of a velocity-azimuth display (VAD) scanning technique for $n = 12$ beam directions. The laser beam of the Doppler lidar points upwards with a constant elevation angle ε and rotates around the vertical Z with configurable azimuth angles α. The red volumes symbolize an emitted "light"-disturbance of a specified period of time (i.e. pulse width Δt) travelling along the line-of-sight (LOS). R is the range of the measurement along LOS and Δr defines the pulse length. The latter is related to the pulse width via $\Delta r = c \cdot \Delta t / 2$, with c denoting the speed of light.

2.1.1 1.5 µm Doppler lidar

The DL emits laser pulses in the near infrared which scatter off particles suspended in the atmosphere such as aerosols and clouds. Data availability is therefore linked to the presence of such particles. The backscattered light has a Doppler shift due to the movement of these particles which can be detected by optical heterodyning in the receiver. Assuming that the target is following the wind, the horizontal wind vector can be determined from the measured line-of-sight (LOS) Doppler wind values. The technical specifications of the StreamLine Doppler lidar developed by Halo Photonics are listed in Table 1. The pulse repetition frequency (PRF) implies a maximum unambiguous range of about 10 km. For wind measurements, a VAD scan pattern was set-up as illustrated in Fig. 1. The sketch is limited to $n = 12$ beam pointing directions or rays, however, the measurement scan pattern was using $n = 24$ azimuthal positions with a constant elevation angle $\varepsilon = 75°$. Measurements of Doppler velocities $V_r(R, \alpha, t)$ were thus made along a circle at $15°$ constant intervals of azimuth α. R indicates the range of the measurement, i.e. the distance of the backscattering volume along LOS, and t denotes the time of the measurement. For each of the 24 rays a total of 75 000 laser shots have been emitted. The dwell time for one ray was about 5 s. Taking the time for the scanner movement into account, one full scan lasted about 3 minutes. For $\varepsilon = 75°$, the range gate length

of $\Delta R = 48$ m translates to a vertical resolution of about $\Delta Z = 46$ m.

2.1.2 482 MHz radar wind profiler

While the measurement principle of the RWP is also based on the Doppler effect, the significantly longer wavelength of 62 cm makes it possible to obtain measurable echoes from both the particle-free (clear) atmosphere due to fluctuations of the refractive index as well as from the particle-laden atmosphere (clouds with sufficiently large particles and precipitation), see e.g. Gossard and Strauch (1983); Gage et al. (1999). Therefore, wind information can almost always be obtained for the entire depth of the troposphere provided the refractive index fluctuations have a sufficient strength at half the radar wavelength.

The passive phased array antenna of the system is designed to steer the beam into five different directions (vertical and four obliques with an elevation angle of $74.8°$). In the operational configuration, the RWP cycles continuously through the four oblique beam directions. The operational set-up uses two different pulse widths to obtain data with different radial resolutions (low and high mode). Eventually, a total of five cycles per mode is used to generate 30 min averaged profiles. The averaging algorithm used is called "consensus averaging" (Fischler and Bolles, 1981; Strauch et al., 1984) and is applied to each beam direction separately. This algorithm facilitates discrimination between "good" and "bad" estimates in the regime of low signal-to-noise ratios (SNR) (Frehlich and Yadlowsky, 1994). For the purpose of this study, only data from the low mode with a pulse width of $\tau = 1000$ ns are considered. RWP low mode measurements are available for a total of 96 range gates extending from 450 m up to 9380 m. The radial and the vertical resolution of one range gate is $\Delta R = 150$ m and $\Delta Z = 145$ m, respectively. The vertical spacing of the range gates due to oversampling with 650 ns is 94 m. A summary of the technical specifications of the 482 MHz RWP is given in Table 1.

2.1.3 RS92-SGP radiosonde

The Vaisala RS92 radiosonde measures vertical profiles of pressure, temperature, and humidity from the ground up to the balloon bursting altitude limit of approximately 40 km. To retrieve the horizontal winds (u, v) based on the change of the sonde position, the RS92 is equipped with a GPS receiver. The noise in the raw U and v winds due to the radiosonde's pendulum-like motion and the noise of the GPS data is reduced by a low-pass digital filter (Dirksen et al., 2014). At Lindenberg, radiosondes are routinely launched four times a day at standard times (00:00, 06:00, 12:00, and 18:00 UTC). With the temporal resolution of the sounding wind data of 40 s, the typical ascent rate of about 5 m s^{-1} leads to a vertical resolution of about 200 m.

2.2 Doppler lidar data processing

The system output quantities relevant for the wind vector retrieval are the estimates of Doppler velocity $V_r(R, \alpha, t)$, and the corresponding signal-to-noise ratio $SNR = S / N$, where S is the average signal power and N the average noise power (Frehlich and Yadlowsky, 1994). The wind analysis is based on the following steps of data processing: (i) SNR-based thresholding for sorting "bad" (noise affected) Doppler estimates from "good" estimates, (ii) calculation of 30 min average Doppler lidar VAD scans to match the temporal resolution of the RWP measurements, (iii) reconstruction of the three vector components u, v, w, (iv) quality check and (v) interpolation of the three vector components from the "Doppler lidar grid" to the "wind profiler grid" to achieve the spatial matching. The latter step, however, is only necessary for the comparison between DL and RWP measurements. Further details will be outlined below.

2.2.1 SNR thresholding technique

The detector signal current in a DL is clearly affected by noise effects, mainly dominated by shot noise from the local oscillator (Frehlich and Kavaya, 1991; Frehlich, 1996). Since the systems operate down to very low SNR conditions, this leads to the occurrence of outliers in the signal properties estimation process ("bad" estimates), which are usually uniformly distributed in frequency over the Nyquist-limited search band (Dabas, 1999). In order to separate between "good" (reliable) and "bad" (unreliable) estimates, a simple SNR-based thresholding technique is a common approach. Depending on the instruments' specific parameters the SNR threshold may vary between different instruments. There are a number of studies focusing on techniques for the determination of reasonable threshold SNR, e.g. Frehlich and Yadlowsky (1994); Dabas (1999). For reliable Doppler velocity estimates with an approximate precision of $< 30\,\mathrm{cm\,s^{-1}}$ the manufacturer of the StreamLine Doppler lidar suggests using a threshold SNR of $-18.2\,\mathrm{dB}$ (0.015), see also Fig. 2c in Pearson et al. (2009). Note that this precision value describes the performance of the Doppler estimator which depends on both the instrument (detector noise) and the natural atmospheric variability within the resolution volume. In order to investigate this threshold two test measurements were made in quiescent atmospheric conditions using a permanent vertical stare configuration. To the extent that it is possible to assume zero atmospheric vertical motion for these cases, the uncertainty in the Doppler estimates is only due to instrumental (noise) effects. The data from these tests reveal that the suggested threshold is apparently a rather conservative choice thereby limiting our data availability: in Fig. 2 the Doppler velocities measured during this test period are plotted against the corresponding value for the parameter "intensity" (SNR + 1, a numerically more convenient quantity). For the range $0.992 < (SNR + 1) < 1.006$ the Doppler velocities
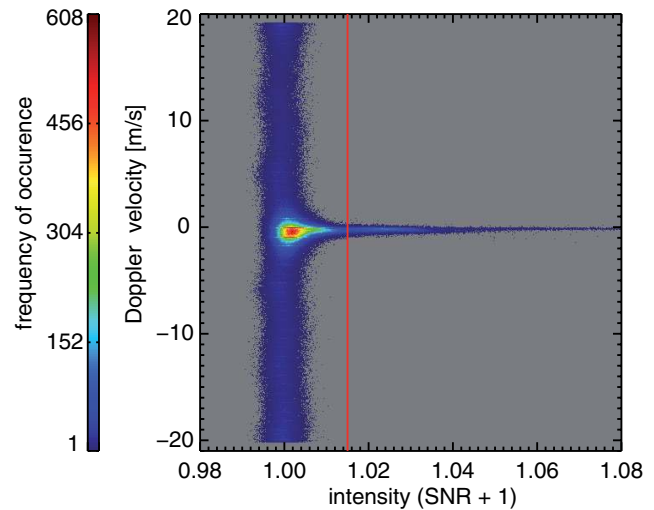

Figure 2. Intensity $(SNR + 1)$ vs. Doppler velocity plot based on Doppler lidar measurements from two different time periods (06:00–07:00 UTC 5 July 2013 and 07:00–08:00 UTC 22 July 2013) which were characterized by quiescent atmospheric conditions, indicated by vertical velocities close to zero. The used Doppler lidar configuration was STARE, i.e. a continuous vertically pointing laser beam. For the range $0.992 < (SNR + 1) < 1.006$ the Doppler velocities are uniformly distributed over the search band $(\pm 19.4\,\mathrm{ms^{-1}})$ indicating a relatively high fraction of "bad" estimates. For $SNR + 1 \geq 1.008$ the Doppler lidar delivers plausible values ("good" estimates). The red line indicates the SNR-threshold $(SNR + 1) = 1.015$ used for the data analysis in the present paper.

are uniformly distributed over the search band which corresponds to the expected statistical distribution of "bad" estimates. Beyond the suggested threshold of 1.015, the Doppler values clustered around zero Hertz are distributed as expected for "good" estimates. The difference between the obvious structural change of the frequency distribution at about 1.008 and the actual threshold of 1.015 is an indication for the possibility to lower the SNR-threshold without risking a significant increase in "bad" estimates. Tests have shown, for instance, that the decrease of the threshold SNR from $-18.2\,\mathrm{dB}$ (0.015) down to $-20\,\mathrm{dB}$ (0.010) would increase the data availability by almost 40 %. However, since the goal of this paper is to assess the accuracy of strictly quality controlled DL wind measurements with respect to the RWP, a refinement of the SNR thresholding technique is left for a future study.

2.2.2 Calculation of 30 min averaged VAD scans

For the intercomparison of winds from the DL and the RWP it is necessary to achieve a match of the temporal resolution between both systems. The DL winds were therefore averaged to 30 min, which corresponds to the operational configuration of the RWP. Two different routes are available for this averaging: one option is to reconstruct first the Carte-

sian vector components u, v, w from each single VAD scan which takes about 3 min (see also Sect. 2.1.1) and then to calculate averaged u, v, w vector components from the ten full VAD scans. The other option is to create mean VAD scans by averaging the ten radial velocity measurements for each azimuth and then reconstructing the u, v, w wind vector components from this single average scan. Here the second way was used since it corresponds best to the "consensus averaging" method employed in the RWP processing.

2.2.3 Wind vector retrieval

The 3-D wind vector profiles are determined on the basis of the 30 min averaged VAD scans described above. Each averaged VAD scan includes temporally averaged Doppler velocities for the 24 different azimuth directions. In principle, radial measurements in three linearly independent directions would be sufficient for a 3-D wind vector reconstruction. However, it will be shown that the use of VAD scans with more than three directions brings considerable benefits in terms of error minimization and in terms of conducting quality checks of the reconstructed 3-D wind vector components, i.e. u, v, w.

Least squares wind components u, v, w using SVD:

Assuming a stationary and horizontally homogeneous wind field, i.e. $\boldsymbol{v}(x, y, z, t) \sim \boldsymbol{v}(z)$, the three wind vector components u, v and w can be obtained by solving the overdetermined linear system

$$\mathbf{A}\boldsymbol{v} = \boldsymbol{V}_r, \tag{1}$$

where $\boldsymbol{v} = (uvw)^{\mathrm{T}}$, $\boldsymbol{V}_r = (V_{r1} V_{r2} V_{r3} \ldots V_{rn})^{\mathrm{T}}$ (with $n = 360°/15° = 24$). The rows of matrix $\mathbf{A}$ are comprised of the unit vectors along the n pointing directions (or rays) with azimuth α_i, $i = 1 \ldots n$, that is

$$\mathbf{A} = \begin{pmatrix} \sin(\alpha_1)\sin(\phi) & \cos(\alpha_1)\sin(\phi) & \cos(\phi) \\ \sin(\alpha_2)\sin(\phi) & \cos(\alpha_2)\sin(\phi) & \cos(\phi) \\ \sin(\alpha_3)\sin(\phi) & \cos(\alpha_3)\sin(\phi) & \cos(\phi) \\ \ldots & \ldots & \ldots \\ \sin(\alpha_n)\sin(\phi) & \cos(\alpha_n)\sin(\phi) & \cos(\phi) \end{pmatrix}. \tag{2}$$

If the azimuth angle α_i (with $i = 1, \ldots, n$) and the elevation angle ϕ are chosen properly (see also Fig. 1), matrix $\mathbf{A}$ is a nonsquare 24×3 matrix with full column rank, that is rank$(\mathbf{A}) = 3$. Equation (1) is clearly overdetermined and can be solved using the method of least squares. The solution is exact when it does exist, otherwise only an approximate solution can be found. A least squares solution $\boldsymbol{v}^\star$ is obtained by minimizing the square of the residual in the 2-norm, i.e. by minimizing $\|\boldsymbol{V}_r - \mathbf{A}\boldsymbol{v}\|_2^2$ (e.g. Strang, 1993). In doing so the least squares solution is given by a standard square (3×3) system

$$\mathbf{A}^{\mathrm{T}}\mathbf{A}\,\boldsymbol{v} = \mathbf{A}^{\mathrm{T}}\boldsymbol{V}_r, \tag{3}$$

where $\mathbf{A}^{\mathrm{T}}$ is the transpose of $\mathbf{A}$. Since $\mathbf{A}$ has full column rank $\mathbf{A}^{\mathrm{T}}\mathbf{A}$ is positive definite and invertible, that is $\boldsymbol{v}$ can be obtained by evaluating the normal equation

$$\boldsymbol{v} = (\mathbf{A}^{\mathrm{T}}\mathbf{A})^{-1}\mathbf{A}^{\mathrm{T}}\boldsymbol{V}_r = \mathbf{A}^+\boldsymbol{V}_r, \tag{4}$$

where $\mathbf{A}^+$ denotes the Moore–Penrose pseudoinverse of $\mathbf{A}$. The normal Eq. (3), however, tends to worsen the condition of the matrix, i.e. cond$(\mathbf{A}^{\mathrm{T}}\mathbf{A}) = (\text{cond}(\mathbf{A}))^2$. For a large condition number, small errors in the (measured) data can produce large errors in the solution. The singular value decomposition (SVD) can be used to solve least squares problem without squaring the condition of the matrix. Employing the SVD, the matrix $\mathbf{A}$ is decomposed using the factorization

$$\mathbf{A} = \mathbf{U}\mathbf{D}\mathbf{V}^{\mathrm{T}}, \tag{5}$$

where $\mathbf{U}$ is an 24×24 orthogonal matrix, $\mathbf{V}$ is an 3×3 orthogonal matrix and $\mathbf{D}$ is an 24×3 diagonal matrix whose elements σ_i are called the singular values of $\mathbf{A}$. Then the least squares solution can be expressed as

$$\boldsymbol{v} = \mathbf{A}^+\boldsymbol{V}_r = \mathbf{V}\mathbf{D}^{-1}\mathbf{U}^{\mathrm{T}}\boldsymbol{V}_r. \tag{6}$$

The advantage of using the SVD in the context of least squares minimization has also been discussed in Boccippio (1995).

Error propagation

Assuming that the Doppler velocity vector $\boldsymbol{V}_r$ has a corresponding known vector of uncertainty, i.e. $\boldsymbol{\sigma}_e = (\sigma_{e1} \sigma_{e2} \sigma_{e3} \ldots \sigma_{en})^{\mathrm{T}}$, the propagation of the radial velocity errors to errors of the components of the wind vector $\boldsymbol{v}$ can be calculated employing the error propagation law. In matrix form, this can be written as

$$\mathbf{C}_{V_r V_r} = \mathbf{A}\mathbf{C}_{vv}\mathbf{A}^{\mathrm{T}} \tag{7}$$

where $\mathbf{C}_{V_r V_r}$ and $\mathbf{C}_{vv}$ denote the variance-covariance matrices of $\boldsymbol{V}_r$ and $\boldsymbol{v}$ defined through the diagonal $n \times n$ matrix

$$\mathbf{C}_{V_r V_r} = \begin{pmatrix} \sigma_{e1}^2 & 0 & \ldots & 0 \\ 0 & \sigma_{e2}^2 & \ldots & 0 \\ \vdots & \vdots & \ddots & \vdots \\ 0 & 0 & \ldots & \sigma_{en}^2 \end{pmatrix} \tag{8}$$

and the 3×3 matrix

$$\mathbf{C}_{vv} = \begin{pmatrix} \sigma_u^2 & \sigma_{uv} & \sigma_{uw} \\ \sigma_{vu} & \sigma_v^2 & \sigma_{vw} \\ \sigma_{wu} & \sigma_{wv} & \sigma_w^2 \end{pmatrix}, \tag{9}$$

respectively. Here, the variance-covariance matrix $\mathbf{C}_{V_r V_r}$ is diagonal, because it is assumed that the errors of the n components of $\boldsymbol{V}_r$ are independent in different directions (Cohn and Goodrich, 2002). It has further been assumed that variances in the elevation and azimuth angles occurring in $\mathbf{A}$ can

Table 2. Decrease of the uncertainties ($\sigma_u, \sigma_v, \sigma_w$) in the 3-D wind vector component retrievals u, v and w with increasing number n of equidistant beam directions per VAD-scan. The values are calculated via Eq. (10) assuming a Doppler velocity uncertainty of $\sigma_r = 10\,\mathrm{cm\,s^{-1}}$ for each beam direction. $\Delta\alpha$ indicates the azimuth resolution.

n	$\Delta\alpha$ (°)	$\sigma_u = \sigma_v$ (cm s^{-1})	σ_w (cm s^{-1})
3	120	31.5470	5.97717
4	90	27.3205	5.17638
6	60	22.3071	4.22650
12	30	15.7735	2.98858
18	20	12.8790	2.44017
24	15	11.1536	2.11325
36	10	9.10684	1.72546

be neglected. For a more detailed discussion of the derivation of the error propagation law in matrix form the reader is referred to Arras (1998), Tellinghuisen (2001) and Boccippio (1995).

The uncertainties σ_u, σ_v and σ_w of the retrieval for u, v, w can be calculated by evaluating the square roots of the diagonal elements of $\mathbf{C}_{vv}$. Using again the notation of the Moore–Penrose pseudoinverse $\mathbf{A}^+$ of matrix $\mathbf{A}$ it is shown in Appendix A that rearranging terms in Eq. (7) yields

$$\mathbf{C}_{vv} = \mathbf{A}^{-1}\mathbf{C}_{V_r V_r}(\mathbf{A}^{-1})^{\mathrm{T}}. \tag{10}$$

In the least square problem described above the measured radial velocities for each beam direction have a precision of $\sigma_{ei} < 30\,\mathrm{cm\,s^{-1}}$ with $i = 1,\ldots,n$ (see Sect. 2.2). Taking error propagation into account one obtains a precision of $\overline{\sigma}_{ei} < 10\,\mathrm{cm\,s^{-1}}$ for each beam direction from a full 30 min averaged VAD scan. Then, setting $\overline{\sigma}_{e1} \equiv \ldots \equiv \overline{\sigma}_{rn} \equiv \overline{\sigma}_e < 10\,\mathrm{cm\,s^{-1}}$ we find by evaluating Eq. (10) by means of SVD that

$$\mathrm{diag}\,\mathbf{C}_{vv} = (124.4, 124.4, 4.5). \tag{11}$$

Eventually, calculating the square roots of the diagonal elements of $\mathbf{C}_{vv}$ yields

$$\sigma_u = \sigma_v < 11.15\,\mathrm{cm\,s^{-1}} \text{ and } \sigma_w < 2.11\,\mathrm{cm\,s^{-1}}. \tag{12}$$

which describes the propagation of the errors in the radial measurements to the wind vector components due to geometry. Note that this assumes the exact validity of Eq. (1), which means that the homogeneity assumption is exactly fulfilled. Possible effects of deviations from this assumption are discussed below.

Finally, the above described approach is used to study the variation of the retrieval uncertainties depending on the variation of the number of beam directions per VAD scan. Table 2 shows that with increasing number of beam directions

the uncertainties can be reduced, most obviously the uncertainty σ_w of the vertical wind component w. Thus it can be concluded that a VAD scan is not only useful for horizontal wind vector reconstructions but also for the determination of the vertical wind provided the number of beam directions is high enough. However, it should be kept in mind that the reconstructed w would differ from direct stare measurements because of the horizontal homogeneity assumption.

2.2.4 Quality assurance

The wind retrieval algorithm described in Sect. 2.2.3 is based on horizontal homogeneity of the wind field within the scanning volume. This is a necessary assumption to devise a closed set of equations for the unknown wind vector components u, v and w. Furthermore, the retrieval through the pseudoinverse needs to be numerically stable, which is not always guaranteed when only a subset of radial measurements is available due to atmospheric variability in backscattering. In this section two parameters are described which have been used for conducting quality assurance of the retrieved winds.

Test of horizontal homogeneity

It is well known that the wind field is not always horizontally homogeneous (Goodrich et al., 2002; Cheong et al., 2008), this is mainly due to convection, gravity waves or shear induced turbulence. Characteristic temporal and spatial scales for turbulence are $T = 10\,\mathrm{s}$ and $L = 1\,\mathrm{m}$. For thermally induced convective processes we typically have $T = 5\,\mathrm{min}$ and $L = 500\,\mathrm{m}$. Thus, with reference to a full DL scan lasting about 3 min and with a scanning circle having height dependent diameters d_C of about $d_C \sim 300\,\mathrm{m}$ at an altitude of $\sim 550\,\mathrm{m}$ and $d_C \sim 5360\,\mathrm{m}$ at $\sim 10\,\mathrm{km}$ it is often the case that due to the occurrence of turbulent motions there are rapid wind fluctuations along the scanning circle and accordingly the assumption of a horizontally homogeneous wind field is not fulfilled. For that reason 3-D wind vector retrievals based on measurements collected during such inhomogeneous wind field conditions have to be flagged. The strategy used to identify wind retrievals during such inhomogeneous wind field conditions is described next.

For a horizontally homogeneous wind field, the reconstruction of the mean wind u, v, w from radial velocities obtained by a VAD scan scheme can be regarded as a sine wave fitting (Banakh and Smalikho, 2013). The overall quality of the fit to this sine wave model is affected by deviations from these homogeneous conditions and can be measured by the coefficient of determination R^2 defined through

$$R^2 = 1 - \sum_i (V_{ri} - \widetilde{V}_{ri})^2 \Big/ \sum_i (V_{ri} - \overline{V}_r)^2, \tag{13}$$

with $\overline{V}_r = \sum_i V_{ri}$ and $\widetilde{V}_{ri}$ denoting the radial velocities from the "sine wave fit". R^2 is used as a quality control parameter for u, v and w reconstructions.

For the analysis in the present paper a reconstructed 3-D wind vector has been rejected if $R^2 < 0.95$. An interpretation of this value is that 95 % of the variations of the averaged VAD scan Doppler velocities are due to variations in the beam direction α_i and only 5 % of the variations have to be explained by other factors. For an exact horizontally homogeneous wind field and exact Doppler velocity estimates the VAD Doppler velocity variations are solely caused by the variation in the beam direction α_i. Thus, with the requirement $R^2 < 0.95$ it is possible to identify such VAD scans for which the assumption of a horizontal wind field is only partially fulfilled. It is important to point out that the selection of $R^2 < 0.95$ as a strict data rejection threshold is only based on our experiences and therefore ad hoc. Further work is required to investigate whether homogeneity can be restored in the statistical sense by judicious temporal averaging.

Collinearity diagnostics

The requirement of $R^2 \geq 0.95$ turned out to be only a necessary condition for "good" wind vector reconstructions, since the retrieval needs also to be numerically stable with respect to small errors in the input or, in other words, well-conditioned. This is achieved when the degree of collinearity among the Doppler velocity measurements used for the retrieval is relatively weak, since a robust linear independence of the sampling directions is an essential prerequisite for the reconstruction of the wind vector. Multicollinearity describes a high linear relationship among one or more independent variables (Belsley et al., 1980) and it is also a well known issue in regression analysis that multicollinearity may result in parameter estimates with incorrect signs and implausible magnitudes (Mela and Kopalle, 2002) or may affect the regressions' robustness, i.e. small changes in the data may result in large changes in the parameter estimates (Boccippio, 1995). Thus, multicollinearity makes the parameter estimates less reliable and has to be detected to exclude erroneous (unphysical) u, v, w retrievals from VAD scans. In the context of least squares parameter estimation from a VAD scan, a high degree of multicollinearity may occur in situations when there are large azimuthal gaps in the measurements due to limited or non-existing backscattering targets within the atmosphere. This issue was recognized by Matejka and Srivastava (1991) in the VAD analysis of single-Doppler radar data.

The condition number (CN) is a parameter that can be used for the detection of collinearity. If the condition number of the problem is small (close to 1) the degree of collinearity is relatively weak. In contrast, a large condition number is an indicator for a strong collinearity among the variables. Boccippio (1995) employed the condition number for an analysis of the VVP (volume velocity processing) retrieval method and identified condition numbers around 9–12 as a threshold indicating collinearity in the regression. In Wissmann et al. (2007) values for CN of 10 and 30 are mentioned to indi-
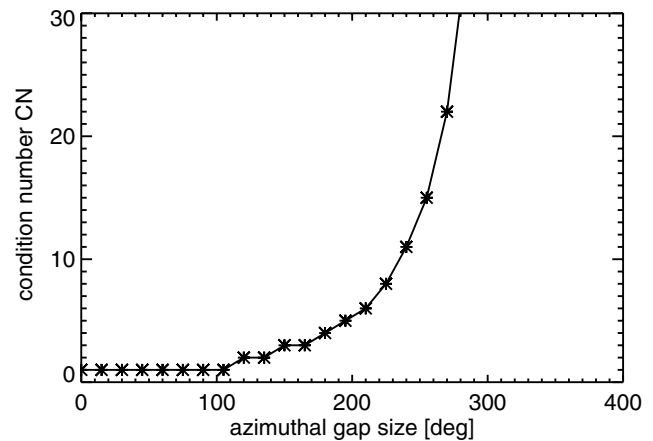

Figure 3. Condition number (CN) vs. azimuthal gap size for a VAD scan with 15° intervals of azimuth α and a constant elevation angle $\varepsilon = 75°$.

cate medium and serious degrees of multicollinearity, respectively.

For the collinearity diagnostics the approach as described in Boccippio (1995) has been adopted. In particular, CN is calculated based on the standardized (scaled) data matrix $\mathbf{Z} = \mathbf{A}\mathbf{S}$, where

$$\mathbf{S} = \text{diag}(s_1, s_2, s_3) \text{ with } s_i = \left(A_i^{\mathrm{T}} A_i\right)^{-1/2}. \tag{14}$$

Here, $\mathbf{A}_i$ denote the columns of matrix $\mathbf{A}$, i.e. $\mathbf{A} = [A_1 A_2 A_3]$. If the singular value decomposition of $\mathbf{Z}$ is used, the condition number CN($\mathbf{Z}$) can be calculated as

$$\mathrm{CN}(\mathbf{Z}) = \frac{\eta_{\max}}{\eta_{\min}}, \tag{15}$$

where η_i ($i = 1, 2, 3$) are the singular values of $\mathbf{Z}$. The standardization of the data matrix is recommended by Belsley (1991). For further details concerning the scaling problem of the condition number the reader is referred to Wissmann et al. (2007). Figure 3 indicates an increase of the condition number with increasing azimuthal gaps for a VAD scan configuration. For a gap size of 280° the condition number is CN = 30 which according to Wissmann et al. (2007) indicates severe collinearity. In such a case, all radial measurements stem from only one quadrant of the scan. For the quality control used in the present analysis a CN threshold of 10 has been used. This means that 3-D wind vector reconstructions obtained from VAD scans with azimuthal gaps $\geq 240°$ have been rejected. Future work is required to investigate to what extent this rather conservative threshold can be relaxed.

Example

An example of the above-described strategy of quality control is illustrated in Fig. 4. The 30 min averaged wind profiles shown here are based on DL measurements from 22
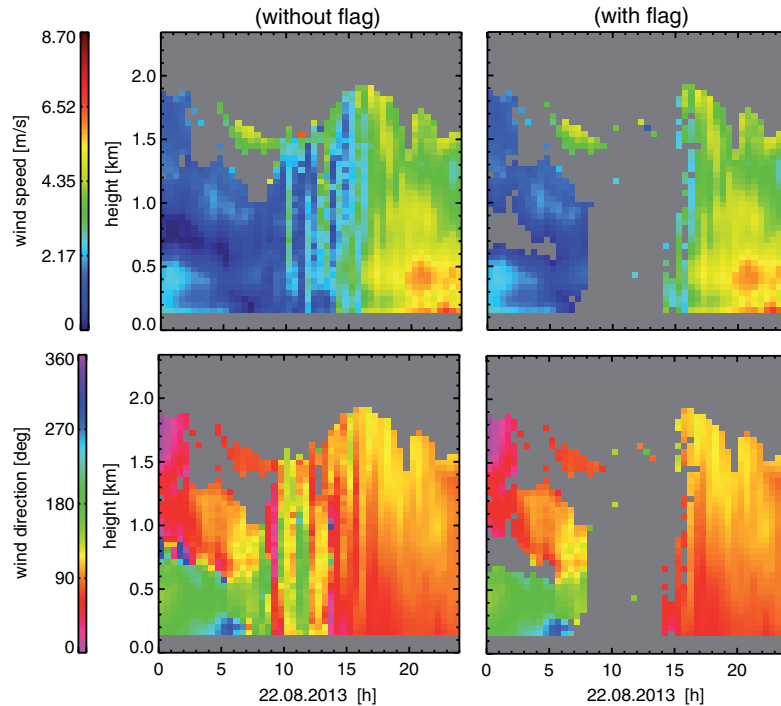
Figure 4. Left column: example of non-quality assured wind profile retrievals (top: wind speed, bottom: wind direction) from Doppler lidar measurements for a typical summer day (22 August 2013). Each profile represents a 30 min average of VAD Doppler lidar measurements with one scan lasting about 3 min. Right column: same wind retrievals as shown in the left column but where profiles with test parameters $R^2 < 0.95$ and CN > 10 have been discarded.

August 2013, which was a typical summer day with a pronounced diurnal cycle of a convective boundary layer (CBL). The plots on the left show 30 min averaged vertical profiles of wind speed and wind direction, estimated from Eq. (6). The plots on the right show the corresponding wind profiles after additional consistency checking. The parameters R^2 and CN for each of the retrievals are shown in Fig. 5. It can be observed that profiles between 08:00 UTC + 02:00 and 14:00 UTC + 02:00 were rejected. This is mainly due to values for $R^2 < 0.95$ which can be attributed to the inhomogeneous flow occurring within a well established CBL. Figure 6 illustrates this situation by showing VAD fits for both homogeneous and inhomogeneous situations.

With regard to the condition number, Fig. 5 shows only a few cases with CN > 10, mostly in the upper part of the boundary layer where azimuthal gaps within the VAD scan are more likely due to a low particle density. Even if multicollinearity is a rare problem there is a need to define a CN threshold (here CN > 10) as an additional condition. An instructive example to illustrate this need is given in Fig. 4, which shows three mean VAD scans obtained between 11:03 UTC and 11:32 UTC for three adjacent range gate heights $h_1 = 1460.48$ m, $h_2 = 1506.84$ m and $h_3 = 1553.21$ m along with the corresponding consistency check parameters R^2 and CN. It is noticeable that the sine wave fit at h_3 has a much greater amplitude compared to h_2 and h_1. Since the ampli-

tude is a measure for the wind speed, this would imply much stronger winds at h_3 than at the lower heights at h_2 and h_1. This data point corresponds to the "red pixel" at the height gate of 1553.21 m in Fig. 4. Obviously, this wind is implausible. A detailed analysis of the mean VAD-scan indicates that the sine-wave fit of the radial measurements is nearly perfect in this case, with $R^2 = 0.98$, see Fig. 7. However, radial wind data are only available in five almost contiguous directions which are only spanning a sector of 75°, namely from 315° to 30° in azimuth. Equivalently, this leaves an azimuthal gap of 285° where no radial winds are available. In general it seems to be possible that a valid wind vector can also be retrieved in this setting, however even small errors in the radials are obviously amplified up to the point where the end result is grossly in error. The condition number of CN = 22 clearly reflects the rather large gap in the radial velocity measurements and the high degree of collinearity for this VAD scan.

2.2.5 Data preparation for intercomparisons

The Doppler lidar measurements obtained with our configurations have a vertically finer resolution than the measurements of the RWP. For the purpose of intercomparison between Doppler lidar-, RWP- and radiosonde measurements it is therefore useful to define a common reference grid to make the values comparable. Since the interpolation from a
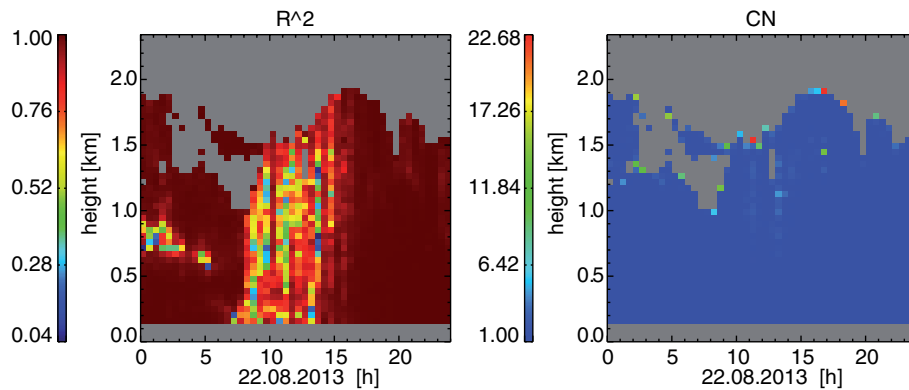
Figure 5. Calculated quality control parameters for the wind profiles shown in Fig. 4. R^2 is the coefficient of determination which provides a measure for the "goodness" of sine wave fit into the VAD Doppler velocity measurements. To ensure that the horizontal homogeneity assumption inherent to the wind vector retrieval is fulfilled, wind vector reconstructions with $R^2 < 0.95$ are classified as non reliable. Additionally, retrievals with $R^2 \geq 0.95$ are only valid for a condition number CN ≤ 10.

coarser grid to a finer grid is naturally more problematic than vice versa, we have chosen the wind radar grid as the reference grid for our studies. For the interpolation of the 30 min averaged 3-D wind vector components u, v, w from the finer Doppler lidar (or finer radiosonde) grid to the coarser and equidistant grid of the RWP, a cubic spline interpolation was used. In detail this means that between two grid points of the finer grid a smooth function is determined first, which passes exactly through those points. Between two grid points of the finer grid, this smooth function is evaluated at the coarser grid point to get the interpolated value. The procedure achieves the vertical matching of the profiles required for the intercomparison. However, the horizontal separation of the RS profile due to the wind-induced drift of the in situ sensor has not been taken into account. This introduces an error of representativity as an additional contribution to the RS-DL differences. For the mean ascent rate of the RS, the top of the ABL is typically reached after less than 10 min. For a mean wind speed of $10 \, \mathrm{m \, s^{-1}}$ this leads to a maximal horizontal separation of only 6 km. It is assumed that the representativity difference due to this horizontal separation of sampling volumes is tolerable, however a refined study can certainly use the sondes GPS position for an additional stratification of the data set. With respect to temporal matching, each of the profiles is assigned to a uniform UTC based time grid.

3 Analysis/statistics

In this section the statistics of 1-year-long DL measurements for wind speed and wind direction are presented. The results are verified with corresponding measurements obtained with a collocated 482 MHz RWP and measurements from the RS92-SGP radiosonde launched at the same observation site.

3.1 Data availability

For the period under investigation, the maximum number of 30 min averaged wind profiles is 17568 provided the measurement conditions are perfect in terms of optical conditions (clouds and aerosols) and wind field structure (homogeneous vs. non-homogeneous). Clearly, measurement conditions are not always ideal as shown in Fig. 8 which naturally leads to a decrease in the number of quality controlled data. At the lowest level of the reference grid (i.e. 552 m) a total of 9798 ($\sim 56\%$) averaged values could be obtained whereas these numbers decrease to 697 ($\sim 4\%$) at 2056 m. The decrease of data availability continues further upwards and approaches less than 10 ($\sim 0.06\%$) for altitudes higher than 7038 m. This strong decrease of data availability with height reflects the vertical distribution of aerosol and cloud particles within the atmosphere. This is the main reason why the IR Doppler lidar is mainly used for wind measurements within the ABL. Of course, these limitations of DL data availability need to be taken into account for the generation of a representative wind climatology.

Also shown in Fig. 8 is the data availability obtained with the collocated RWP (low mode) and those from routine RS launches. Not surprisingly, both measurement systems provide higher data availabilities within the free atmosphere than the DL. The decrease of RWP data availability with height is related to the profile of the structure constant of refractive index turbulence (C_n^2) (Atlas, 1990). For the two comparisons, i.e. DL vs. RWP (hereafter referred to as DLWR) and DL vs. RS (hereafter referred to as DLRS), we only use the subset where valid data are available from both systems, i.e. the intersection of the respective data sets. Figure 8 gives an overview of to what extent this further decreases the data availability for our statistical analysis. To get representative statistical results for a "1-year comparison" the comparisons are restricted to heights up to
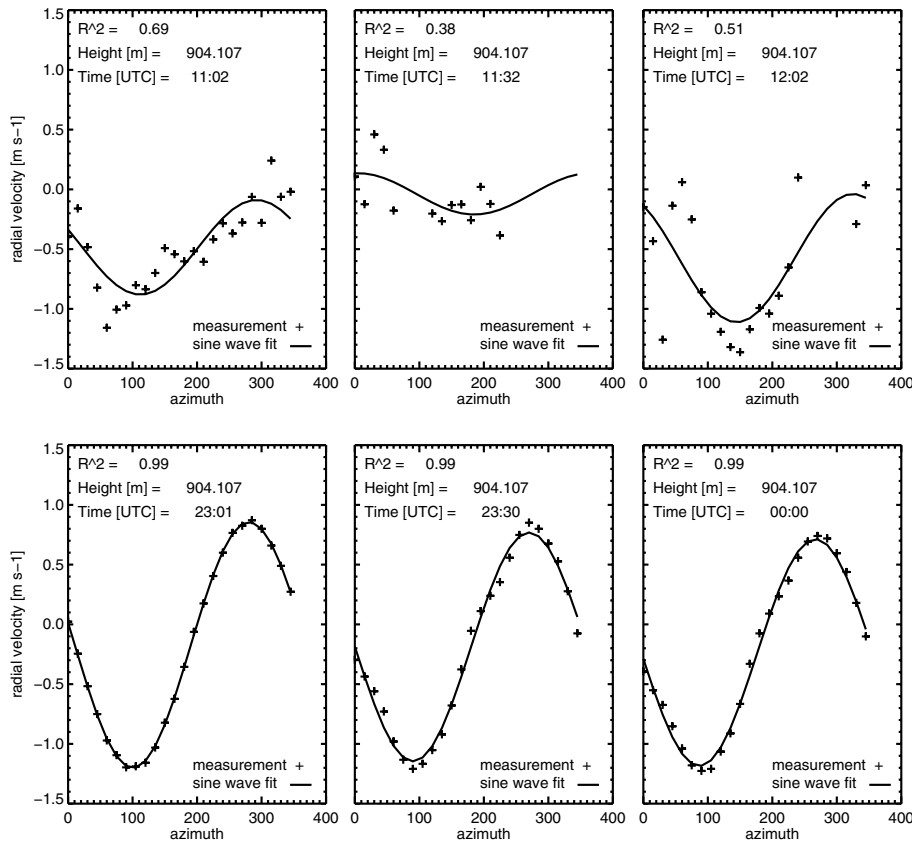
Figure 6. Examples of single sine wave fits into 30 min averaged VAD scans used to reconstruct the 30 min averaged wind profiles shown in Fig. 4 at 904 m height with the time stamps 11:02, 11:32 and 12:02 UTC (upper row) and the three time stamps 23:01, 23:30 and 00:00 UTC (lower row). The measurements in the upper line were obtained during a well evolved CBL where horizontal homogeneous conditions were not met, which is also reflected in the low R^2 values. The measurements in the lower row were obtained during stable atmospheric conditions at night. Here, the high values for R^2 indicate that the assumption of a horizontally homogeneous wind field is better fulfilled.

~ 2800 m for the comparison DLWR and up to ~ 1300 m for the comparison DLRS, which guarantees that the sample size is > 200. For this data basis the precision $\Delta \overline{v}_{\text{speed}}$ of a calculated quasi-annual wind speed is on the order of about $\Delta \overline{v}_{\text{speed}} = 7 \times 10^{-4} \, \text{m s}^{-1}$

3.2 DLWR and DLRS comparisons

The calculated statistics in this section serve as a diagnostics to obtain insights into the validity of the 3-D wind vector retrievals from DL measurements. Abbreviations used for the error scores are: ME (mean error), MAE (mean absolute error) and RMSE (root mean squared error).

3.2.1 Scatter plots

For a first overview, the 30 min averaged lidar winds are compared against 30 min averaged RWP winds on the one hand and against temporally matched radiosonde winds on the other for the full period and all heights. The corresponding scatter plots are shown in Fig. 9 for wind speed and wind direction, respectively. Regarding the wind speed it can be

observed that for both comparisons (DLWR and DLRS) the majority of data points fall very close to the identity line which indicates a generally good agreement of the respective data samples. In more detail, however, the correlation (m) indicates a slightly better linear relationship between RS and DL wind speeds ($m = 0.99$) than between RWP and DL wind speeds ($m = 0.97$). This seems to be mainly due to the better agreement of higher wind speeds (e.g. $> 20 \, \text{m s}^{-1}$) for the DLRS comparison than for the DLWR comparison.

Additionally a greater spread of data pairs around the identity line is observed for the DLWR comparison than for the DLRS comparison. However, the respective RMSE scores indicate better agreement for the DLWR comparison than for the DLRS comparison. Since the RMSE gives a high weight to large errors, the lower RMSE value for the DLWR comparison also indicates that the largest differences occur between the Doppler lidar and radiosonde data. Regarding the wind direction the dots of a huge number of data pairs are concentrated around the identity line and thus likewise indicate good agreement for both comparisons. However, the dots of a small fraction of data pairs are somewhat widely spread
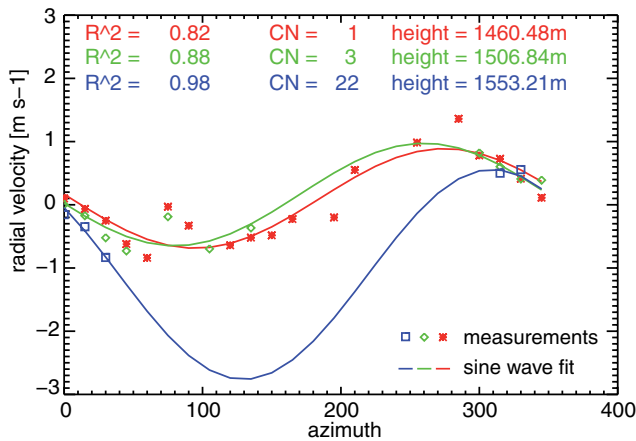
Figure 7. Examples of three sine wave fits used to reconstruct the 30 min averaged wind profiles shown in Fig. 4 at the three adjacent heights $h_1 = 1460.48\,\mathrm{m}$, $h_2 = 1506.84\,\mathrm{m}$ and $h_3 = 1553.21\,\mathrm{m}$ for the single time stamp 12:02 UTC. Additionally for each fit the quality control parameters R^2 and CN are also given. The sine wave fit at h_3 has a high R^2 but due to the large azimuthal gap size within the measurements the condition number CN is relatively high, indicating a high degree of multicollinearity. The latter results in implausible magnitudes of the wind speed yielding unphysical vertical gradients in the wind speed field (see also the outstanding red pixel in the wind speed profile shown in Fig. 4 at the time stamp 12:02 UTC).

and indicate a weaker relationship between measured wind directions. We also find that this is more pronounced for the DLWR comparison than for the DLRS comparison. Note that the clustered data points around 360° at both the horizontal and vertical axis are due to the 2π-periodicity of azimuth.

3.2.2 Annual mean wind profiles

A good agreement in the statistics of the Doppler lidar-, radar wind profiler- and radiosonde measurements is also reflected in the annual mean of the measured vertical profiles for wind speed and direction shown in Fig. 10.

Regarding the DLWR comparison the ME for the wind speed changes a little in sign with varying height up to about 1800 m, whereas the range of speed variations is from $-0.2\,\mathrm{m\,s^{-1}} < \mathrm{ME} < 0.3\,\mathrm{m\,s^{-1}}$. Above 1800 m the ME is always positive and increases from $\sim 0\,\mathrm{m\,s^{-1}}$ at 1800 m up to $0.2\,\mathrm{m\,s^{-1}}$ at about 2500 m. Thus, using the RWP measurements as a reference a systematic difference indicating a slight overestimation of DL wind speeds can be identified for altitudes higher than 1800 m. The reason for this difference is unclear. It is probably also justified to take the possibility of a small range dependent bias in the RWP data into account, which could be further investigated with a long-term RWP-RS intercomparison. Additionally, a sign change of ME is observed for heights below 1800 m in both the DLWR and DLRS comparisons. This small effect is likely due to a hardware issue in the DL that was unfortunately only detected and
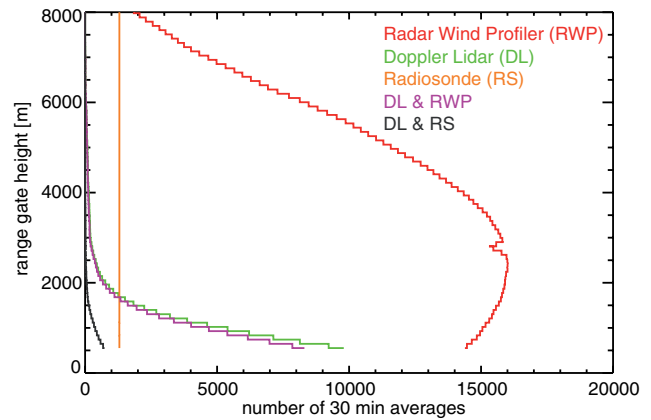

Figure 8. Overview of the data availability from 1-year measurements with Doppler lidar (DL), radar wind profiler (RWP) and radiosonde (RS). Data availability refers to 30 min averaged profiles for wind speed and direction. The number of data used for the DLWR comparison is a subset of data indicated by DL & RWP where both systems provide valid data at the same time. The graph denoted with DL & RS reflects a subset of data where the DL and RS provide valid data at the same time, which have been used for the DLRS comparison.

fixed after the campaign. Concerning the annual mean wind direction there is also a generally good agreement between DL and RWP measurements. Here the mean differences mostly vary between $\pm 1°$. With regard to the error scores MAE and RMSE, the DL and RWP measurements agree in wind speeds mostly within a range of about $0.3\,\mathrm{m\,s^{-1}} < \mathrm{MAE} < 0.5\,\mathrm{m\,s^{-1}}$ and $0.5\,\mathrm{m\,s^{-1}} < \mathrm{RMSE} < 0.7\,\mathrm{m\,s^{-1}}$. For the wind direction $3° < \mathrm{MAE} < 4°$ and $5° < \mathrm{RMSE} < 10°$. The small differences between the MAE and RMSE ranges for the wind speed additionally indicate that there is some variation in the magnitude of the errors but large errors can be ruled out in all likelihood. This is in contrast to the slightly larger differences between the MAE and RMSE ranges for the wind direction at low range gate heights, suggesting that here larger errors occur.

Regarding the DLRS comparison we observe a smaller bias $(-0.2\,\mathrm{m\,s^{-1}} < \mathrm{ME} < 0.1\,\mathrm{m\,s^{-1}})$ below 1500 m than in the DLWR comparison. The verification scores MAE and RMSE, however, are somewhat larger, i.e. $0.5\,\mathrm{m\,s^{-1}} < \mathrm{MAE} < 0.7\,\mathrm{m\,s^{-1}}$ and $0.7\,\mathrm{m\,s^{-1}} < \mathrm{RMSE} < 0.9\,\mathrm{m\,s^{-1}}$ for wind speed and $5° < \mathrm{MAE} < 6°$ and $9° < \mathrm{RMSE} < 12°$ for wind direction.

The presented long-term intercomparison results confirm the main findings of previous intercomparison results (see Sect. 1) obtained from short-term measurement periods. The good agreement also indicates a rather small instrument error in all systems, since the methodology of the comparison was targeted at minimizing the sampling error by minimization of both the temporal and spatial separation (about 30 m) between the Doppler lidar and the radar wind profiler.
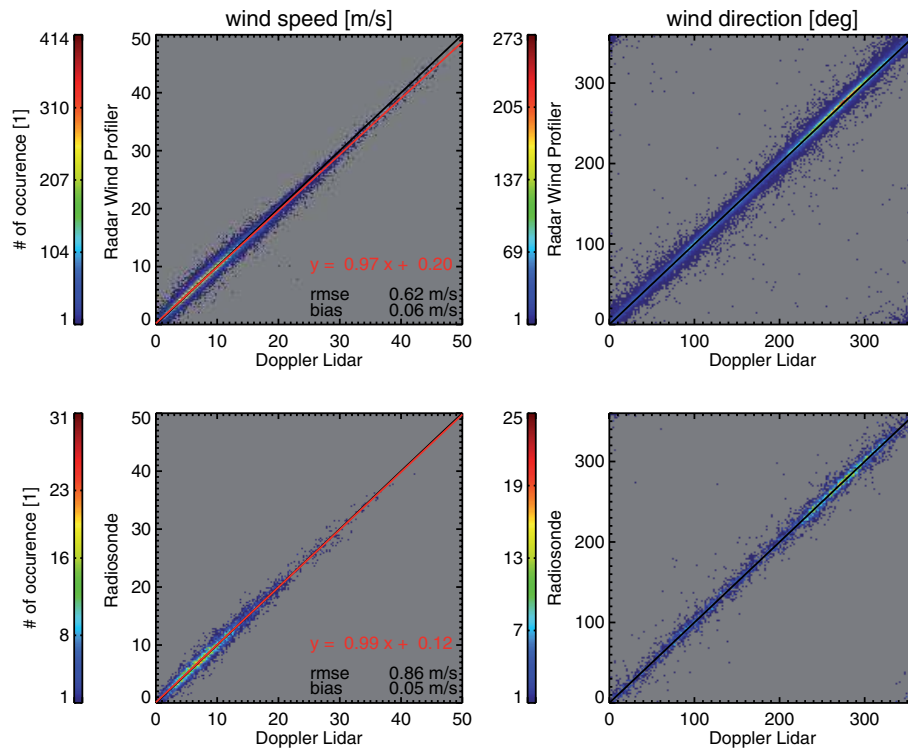
Figure 9. Top: scatter plots of 1-year 30 min averaged horizontal wind speed and direction from the Doppler lidar and 482 MHz radar wind profiler measurements (DLWR). Bottom: scatter plots of 1-year 30 min averaged horizontal wind speed and direction from Doppler lidar and radiosonde (DLRS). Top and bottom: the scatter plots include measurements from all heights. The red line indicates the identity line.

4 Range aliasing effects for smaller SNR-thresholds

The SNR-threshold of −18.2 dB (0.015) is a rather conservative threshold, with the consequence that a huge amount of "good" estimates are rejected. It can therefore be assumed that smaller SNR-thresholds can possibly also be used. An analysis of the Doppler lidar measurements based on an SNR-threshold < 0.015 revealed an interesting type of "gross error", which was not observed when employing the conservative SNR-threshold = 0.015. In radar meteorology, this type of "gross error" is well known as range ambiguity (or range aliasing). This occurs if the atmospheric backscattering at altitudes > Z_{max}, where Z_{max} defines the maximum unambiguous range determined by the pulse repetition frequency and the speed of light c via $PRF_{max} = c/(2Z_{max})$ is stronger than the backscattering in the equivalent unambiguous height range.

In such cases, the range of the backscattering target is incorrectly assigned. The received echo is not associated with the pulse just transmitted, but with the previous pulse. Figure 12 gives an illustrative example of such a range aliasing effect in the DL data, which could be uniquely detected by comparing the lidar measurements with RWP data. Shown are DL and RWP (high and low mode) wind profiles for three different times (11:00, 11:30 and 12:00 UTC). The low mode (higher resolution) profile of the RWP covers a height range

from about 500 m up to about 7 km, whereas the high mode (lower resolution) profile provides data between 4 and 13 km height. Both modes have a sufficient low PRF to avoid range aliasing under all practical circumstances. The DL profiles in contrast are limited to the height range below about 1 km. The striking feature in the DL data are the strong northerly winds (in excess of 50 m s^{-1}) which are clearly erroneous in this height band. These are due to second-trip echoes originating from heights of around 11 km which are incorrectly assigned to the height of about 1 km. Note that the maximum unambiguous range of 10 km in the DL is due to the PRF of 15 kHz.

It is important to point out that such "gross errors" can be easily circumvented by changing the PRF in the sense that the maximum unambiguous sampling range is increased. Of course, this also reduces the number of pulses that can be averaged in a given time interval. While this has a slightly negative effect on the performance of the lidar, the avoidance of gross errors due to range-aliasing clearly outweighs the associated minor disadvantage, at least in operational settings.
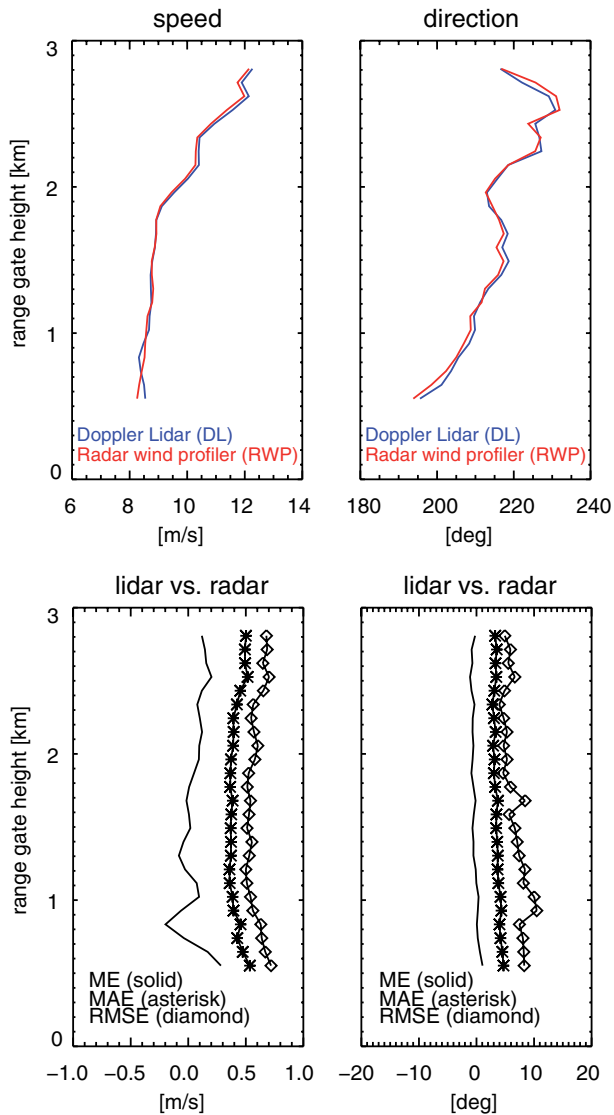
Figure 10. Statistical results of the DLWR comparison. The upper two panels show the annual mean of wind speed and direction obtained from Doppler lidar and wind profiler measurements, respectively. Error bars denoting the precision of the wind speeds in the annual profiles are not shown because of their very low magnitudes (see also the remarks in Sect. 3.1). The lower two panels show the respective verification scores ME (mean error), MAE (mean absolute errors) and RMSE (root mean squared error).

Figure 11. Same as in Fig. 10 but for the DLRS comparison.

5 Conclusions

The capability of a new generation of portable IR Doppler lidar systems for future operational boundary layer wind profiling, complementary to radar profilers, has been tested.

The signal-to-noise ratio threshold of -18.2 dB (0.015) for reliable Doppler wind estimates with a precision of < 30 cm s^{-1} was chosen in a very conservative way.

For the usually employed assumption of a horizontally homogeneous wind field within the volume sampled by the li-
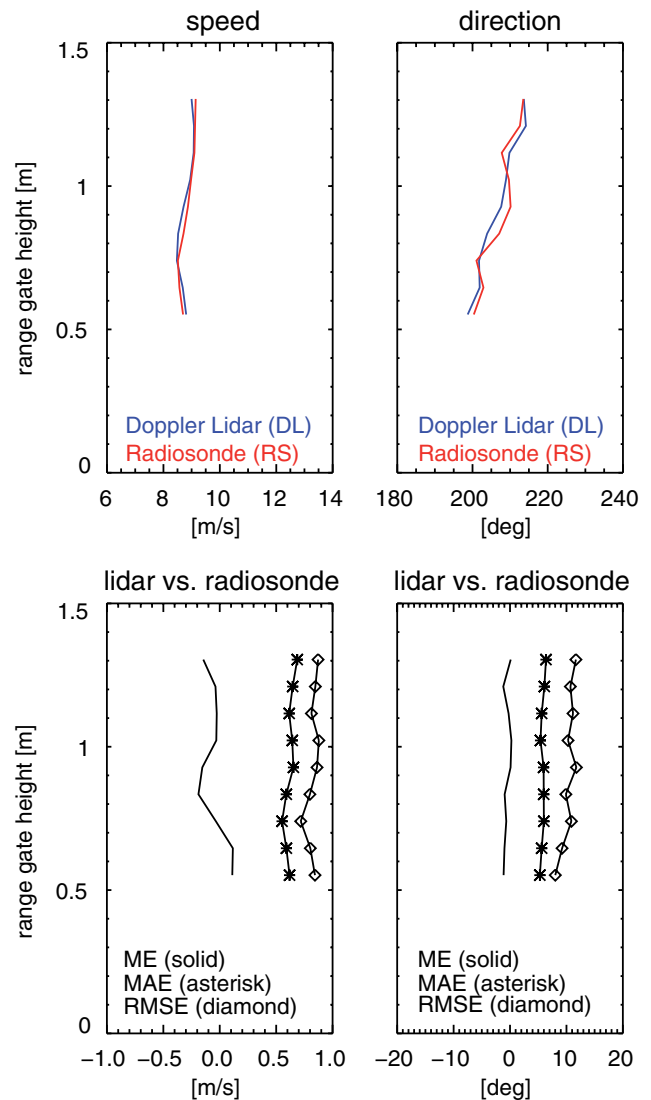
dar, a methodology was developed for the retrieval of the wind vector from a velocity-azimuth display sampling configuration using 24 azimuthal directions with a constant elevation of 75°. The assumptions used for the 3-D wind vector retrievals from Doppler velocity measurements are generally the same for both radar wind profiler and Doppler lidar. One particular advantage of the Doppler lidar is the full hemispheric scanning capability. This allows for more flexible sampling strategies in contrast to most radar profilers, which are restricted to measurements using the Doppler beam swinging mode.

Quality control methods were derived and implemented for testing of the homogeneity assumption used in the retrieval, as well as for the sensitivity of the retrieval against small errors in the input data. In particular, if the number of measurement directions (n) is large enough, the "goodness-

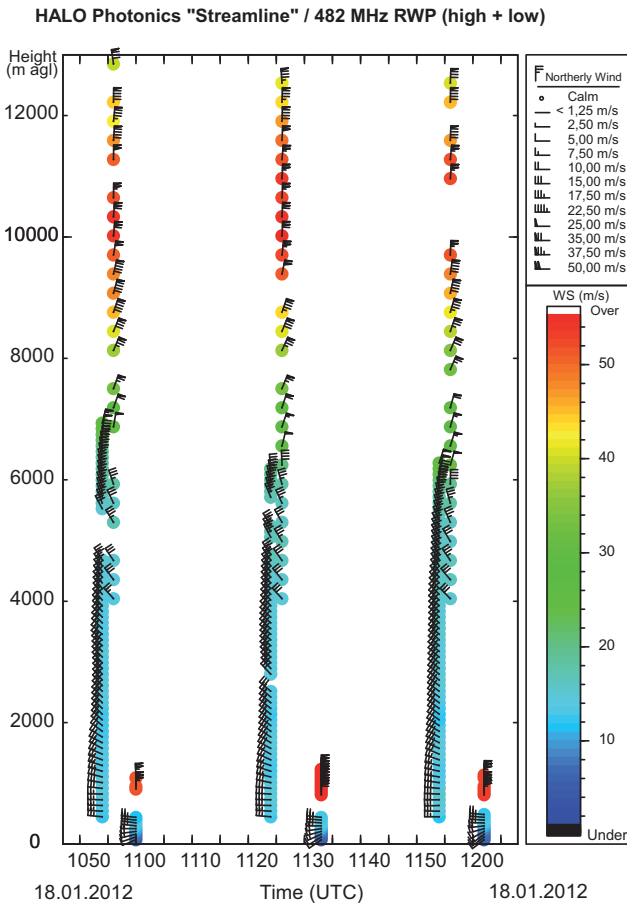**HALO Photonics "Streamline" / 482 MHz RWP (high + low)**

Figure 12. Comparison of three pairs of wind profiles obtained from Doppler lidar measurements and wind profiler measurements, respectively, at three different time slots around 11:00, 11:30 and 12:00 UTC on 18 January 2012. For each time the wind profiler measurements are to the left and the Doppler lidar measurements are to the right. The wind profiler measurements are obtained for two different modes, i.e. a lower one providing wind measurements from 450 m up to 9380 m and a higher one providing additional measurements from about 4000 m up to 13 000 m. The colours indicate the wind speed, the wind barbs give further information on the wind direction.

of-fit" parameter quantified by R^2 turned out to be a useful tool to determine the degree of homogeneity of the wind field. Clearly, non-homogeneous wind fields are more frequently found within the atmospheric boundary layer than in the free atmosphere which renders this test quite important for operational wind profiling with the Doppler lidar.

A second test of a robust linear independence among the Doppler velocity measurements by means of the condition number CN turned out to be useful for detecting erroneous wind estimates which have their origin in a high sensitivity of the retrieval with respect to input errors, a situation which occurs in the case of large measurement gaps within a single VAD scan. This is observed when the backscattering targets are not equally distributed within the VAD-sampled volume, a condition which frequently occurs within the transition zone from the atmospheric boundary layer into the free atmosphere.

In particular, the R^2 quality test with the employed threshold of $R^2 < 0.95$ for bad retrievals discards $\sim$7568 profiles of 17 568 maximum possible profiles over the year, a considerable proportion of Doppler lidar wind retrievals. This was justified because the focus of the investigation was the evaluation of the Doppler lidar accuracy based on strictly quality controlled wind measurements. However, it remains an important topic for future work to find out to what extent both the threshold for R^2 as well as the threshold for the SNR can be relaxed for the sake of a higher data availability without compromising the data quality of the measurements.

Using the processing methodology outlined in the paper, 1-year-long times series of 30 min averaged horizontal wind vector retrievals were calculated from the Doppler lidar and compared with operational radar wind profiler measurements in the atmospheric boundary layer at heights between 500 and 2800 m. These interval limits are determined by the lowest height gate of the 482 MHz wind profiler and the height up to which a sufficient number of Doppler lidar measurements could be obtained to allow for a stable intercomparison statistics. This upper height limit is mainly determined by the natural atmospheric aerosol loading at Lindenberg.

There is a very good agreement in the measurements of both systems, which confirms previous studies that were made on the basis of a much smaller data collection. These results strengthen the basic idea of using DL measurements below 500 m to fill the gap where 482 MHz RWP wind measurements are no longer possible. It is obvious that the strict employment of the two test parameters R^2 and CN was important for the good agreement between Doppler lidar and radar wind profiler measurements.

Appendix A: Error propagation law

If $n > 3$ matrix $\mathbf{A}$ is not invertible. Multiplying Eq. (7) from the left by $\mathbf{A}^T$ and inverting subsequently the expression $(\mathbf{A}^T\mathbf{A})$ one obtains

$$(\mathbf{A}^T\mathbf{A})^{-1}\mathbf{A}^T\mathbf{C}_{V_r V_r} = \mathbf{A}^+\mathbf{C}_{V_r V_r} = \mathbf{C}_{vv}\mathbf{A}^T, \tag{A1}$$

where $\mathbf{A}^+$ denotes the Moore–Penrose pseudoinverse of $\mathbf{A}$ (see also Eq. 4). Next, multiplying with $\mathbf{A}$ from the right yields

$$\mathbf{A}^+\mathbf{C}_{V_r V_r}\mathbf{A} = \mathbf{C}_{vv}\mathbf{A}^T\mathbf{A}, \tag{A2}$$

and inversion of $(\mathbf{A}^T\mathbf{A})$ gives

$$\mathbf{A}^+\mathbf{C}_{V_r V_r}\mathbf{A}(\mathbf{A}^T\mathbf{A})^{-1} = \mathbf{C}_{vv}. \tag{A3}$$

It remains to show that $\mathbf{A}(\mathbf{A}^T\mathbf{A})^{-1} = (\mathbf{A}^+)^T$. First, using the substitution $\mathbf{G} = (\mathbf{A}^T\mathbf{A})^{-1}$ one can write

$$(\mathbf{A}^+)^T = (\mathbf{G}\mathbf{A}^T)^T. \tag{A4}$$

With $(\mathbf{B}\mathbf{C})^T = \mathbf{C}^T\mathbf{B}^T$ and $(\mathbf{D}^T)^T = \mathbf{D}$ (properties of transpose) one can also write

$$(\mathbf{A}^+)^T = (\mathbf{A}^T)^T\mathbf{A}^T = \mathbf{A}\mathbf{A}^T, \tag{A5}$$

and re-substitution yields

$$(\mathbf{A}^+)^T = \mathbf{A}((\mathbf{A}^T\mathbf{A})^{-1})^T. \tag{A6}$$

Making use of $(\mathbf{D}^T)^{-1} = (\mathbf{D}^{-1})^T$ gives

$$(\mathbf{A}^+)^T = \mathbf{A}((\mathbf{A}^T\mathbf{A})^T)^{-1}, \tag{A7}$$

and repeated use of the properties of transpose, yields

$$(\mathbf{A}^+)^T = \mathbf{A}(\mathbf{A}^T(\mathbf{A}^T)^T)^{-1} = \mathbf{A}(\mathbf{A}^T\mathbf{A})^{-1}. \tag{A8}$$

References

Arras, K. O.: An Introduction To Error Propagation: Derivation, Meaning and Examples of Equation $C_Y = F_X C_X F_X^T$, ETH-Zürich, Technical Report No. EPFL-ASL-TR-98-01 R3, doi:10.3929/ethz-a-010113668, (last access: 11 november 2014), 1998.

Atlas, D.: Radar in Meteorology, American Meteorological Society, 45 Beacon Street, Boston, MA 02176, 1990.

Banakh, V. and Smalikho, I.: Coherent Doppler Wind Lidars in a Turbulent Atmosphere, Artech House Publishers, 2013.

Belsley, D.: A guide to using the collinearity diagnostics, Computer Science in Economics and Management, 4, 33–50, 1991.

Belsley, D., Kuh, E., and Welsch, R. E.: Regression Diagnostics: Identifying Influential Data and Sources of Collinearity, John Wiley & Sons, Inc., Hoboken, New Jersey, 1980.

Boccippio, D. J.: A Diagnostic Analysis of the VVP Single-Doppler Retrieval Technique, J. Atmos. Oceanic Technol., 12, 230–248, doi:10.1175/1520-0426(1995)012<0230:ADAOTV>2.0.CO;2, 1995.

Cheong, B. L., Palmer, R. D., Yu, T.-Y., Yang, K.-F., Hoffman, M. W., Frasier, S. J., and Lopez-Dekker, F. J.: Effects of Wind Field Inhomogeneities on Doppler Beam Swinging Revealed by an Imaging Radar, J. Atmos. Oceanic Technol., 25, 1414–1422, doi:10.1175/2007JTECHA969.1, 2008.

Cohn, S. A. and Goodrich, R. K.: Radar Wind Profiler Radial Velocity: A Comparison with Doppler Lidar, J. Appl. Meteor., 41, 1277–1282, 2002.

Dabas, A.: Semiempirical Model for the Reliability of a Matched Filter Frequency Estimator for Doppler Lidar, J. Atmos. Oceanic Technol., 16, 19–28, doi:10.1175/1520-0426(1999)016<0019:SMFTRO>2.0.CO;2, 1999.

Dirksen, R. J., Sommer, M., Immler, F. J., Hurst, D. F., Kivi, R., and Vömel, H.: Reference quality upper-air measurements: GRUAN data processing for the Vaisala RS92 radiosonde, Atmos. Meas. Tech., 7, 4463–4490, doi:10.5194/amt-7-4463-2014, 2014.

Fischler, M. A. and Bolles, R. C.: Random Sample Consensus: A Paradigm for Model Fitting with Applications to Image Analysis and Automated Cartography, Commun. Assoc. Comput. Mach., 24, 381–395, 1981.

Frehlich, R.: Simulation of Coherent Doppler Lidar Performance in the Weak-Signal Regime, J. Atmos. Oceanic Technol., 13, 646–658, doi:10.1175/1520-0426(1996)013<0646:SOCDLP>2.0.CO;2, 1996.

Frehlich, R. and Yadlowsky, M.: Performance of Mean-Frequency Estimators for Doppler Radar and Lidar, J. Atmos. Oceanic Technol., 11, 1217–1230, 1994.

Frehlich, R. G. and Kavaya, M. J.: Coherent laser radar performance for general atmospheric refractive turbulence, Appl. Opt., 30, 5325–5352, doi:10.1364/AO.30.005325, 1991.

Gage, K. S., Williams, C. R., Ecklund, W. L., and Johnston, P. E.: Use of Two Profilers during MCTEX for Unambiguous Identification of Bragg Scattering and Rayleigh Scattering, J. Atmos. Sci., 56, 3679–3691, doi:10.1175/1520-0469(1999)056<3679:UOTPDM>2.0.CO;2, 1999.

Goodrich, R. K., Morse, C. S., Cornman, L. B., and Cohn, S. A.: A Horizontal Wind and Wind Confidence Algorithm for Doppler Wind Profilers, J. Atmos. Oceanic Technol., 19, 257–273, doi:10.1175/1520-0426-19.3.257, 2002.

Gossard, E. E. and Strauch, R. G.: Radar Observations of Clear Air and Clouds, Elsevier, 1983.

Matejka, T. and Srivastava, R. C.: An Improved Version of the Extended Velocity-Azimuth Display Analysis of Single-Doppler Radar Data, J. Atmos. Oceanic Technol., 8, 453–466, doi:10.1175/1520-0426(1991)008<0453:AIVOTE>2.0.CO;2, 1991.

Mela, C. and Kopalle, P.: The impact of collinearity on regression analysis: The asymmetric effect of negative and positive correlations, Appl. Eco., 34, 667–677, 2002.

Pearson, G., Davies, F., and Collier, C.: An Analysis of the Performance of the UFAM Pulsed Doppler Lidar for Observing the Boundary Layer, J. Atmos. Oceanic Technol., 26, 240–250, doi:10.1175/2008JTECHA1128.1, 2009.

Shaw, W., Darby, L., and Banta, R.: A comparison of winds measured by a 915 MHz wind profiling radar and a Doppler lidar, 83rd AMS annual meeting (12th Symp. on Met. Observ. & Instrument.), Long Beach, CA, 9-13 February, P1.8, https://ams.confex.com/ams/pdfpapers/58646.pdf, 2003.

Skolnik, M. I.: Introduction to Radar Systems, McGraw-Hill, 2001.

Strang, G.: The Fundamental Theorem of Linear Algebra, The American Mathematical Monthly, 100, 848–855, 1993.

Strauch, R. G., Merritt, D. A., Moran, K. P., Earnshaw, K. B., and van de Kamp, D.: The Colorado wind profiling network, J. Atmos. Oceanic Technol., 1, 37–49, 1984.

Tellinghuisen, J.: Statistical Error Propagation, J. Phys. Chem. A, 105, 3917–3921, doi:10.1021/jp003484u, 2001.

Wissmann, M., Toutenburg, H., and Shalabh: Role of Categorical Variables in Multicollinearity in the Linear Regression Model, Department of Statistics, University Munich, Germany, Technical Report Number 008, 34 pp., http://nbn-resolving.de/urn/resolver.pl?urn=nbn:de:bvb:19-epu%b-2081-0, last access: 11 november 2014, 2007.